PAPER

Check for updates

Sprayed copper peroxide nanodots for accelerating wound healing in a multidrug-resistant bacteria infected diabetic ulcer†

Ran Zhang,[a] Guhua Jiang,[a] Qianqian Gao,[b] Xiaona Wang,[c] Yilin Wang, [ID][a] Xin Xu,[a] Wenjing Yan[a] and Haijun Shen [ID] *[a]

Vascular dysfunction and bacterial infection are key factors for the non-healing of diabetic ulcers. Growth factors and antibiotics seem to effectively target both issues. However, the short half-life and high cost of growth factors and the antibiotics resistance of bacteria greatly limit their further widespread applications. Novel strategies or agents with both angiogenic and antibacterial activities are urgently desirable. Copper peroxide (CuO_2) nanodots were reported to be decomposed into Cu^{2+} and H_2O_2 under mild acid conditions (pH 5.5). Considering that both decomposed products are acknowledged antibacterial agents (Cu^{2+}, H_2O_2) and angiogenesis activator (Cu^{2+}), we believe that CuO_2 nanodots are suitable for diabetic ulcer treatment because the pathological environment of infected chronic wounds is mildly acidic with pH 5.5–5.6. As expected, *in vitro* experiments showed that CuO_2 nanodots possessed excellent bactericidal properties against *Escherichia coli*, *Staphylococcus aureus*, *Pseudomonas aeruginosa*, and even methicillin-resistant *Staphylococcus aureus* (MRSA). CuO_2 nanodots induced the high expression of hypoxia-inducible factor (HIF-1α) and vascular endothelial growth factor (VEGF) in human umbilical vein endothelial cells (HUVECs), subsequently promoting the cell migration and tube formation for angiogenesis. In particular, CuO_2 nanodots exhibited good dispersibility and sprayable behavior in water. *In vivo* experiments demonstrated that the spayed CuO_2 nanodots in the wound area could effectively combat MRSA, reduce inflammation, promote angiogenesis, and consequently accelerate wound healing. Moreover, the sprayed CuO_2 nanodots in the wound sites caused negligible system toxicity. This study provides proof-of-principle evidence for applying the sprayed CuO_2 nanodots for infected diabetic ulcer treatment.

Introduction

According to the International Diabetes Federation (IDF), the number of diabetics aged 18–99 worldwide (451 million in 2017) is expected to grow to 693 million by 2045.[1] Diabetic ulcers, a devastating chronic complication of diabetes, are characterized by chronic wounds that usually occur on the foot or other skin folds.[2,3] Due to severe pain, ischemia, infection and destruction of deep tissues, about 25% diabetic ulcer patients end up with amputation that results in lifelong disabilities,[4–6] which brings great burden to patients and

society.[7] However, the commonly used hyperbaric oxygen therapy, negative pressure wound therapy and surgical reconstruction of the lower limb blood supply are not ideal. The effective treatment of diabetic ulcers is still a great challenge in clinic.[8–10]

Vascular dysfunction and bacterial infection have been acknowledged as the main reasons for the non-healing nature of chronic wounds in diabetic ulcers. The vascular dysfunction will hinder the transport of nutrients and growth factors and the removal of waste products in the newly formed granulation, forming chronic wounds.[6,11,12] Owing to the delayed healing time and hyperglycemic environment, the wounds will be susceptible to bacterial infections. The virulence factors (such as hemolysin, short chain fatty acids, collagenase and protease) produced by bacterial interactions, in turn, delayed wound healing with severe pain.[8,13] Therefore, enhancing angiogenesis and preventing bacterial infections are critical to accelerate chronic wound healing, which is beneficial for the treatment of diabetic ulcers.[14]

Growth factors and antibiotics seem to meet the above requirements very well, and they have been used to treat

[a]Department of Preventive Medicine and Public Health Laboratory Science, School of Medicine, Jiangsu University, Zhenjiang 212013, China. E-mail: shenhj@ujs.edu.cn
[b]Department of Clinical Laboratory, Affiliated Kunshan Hospital of Jiangsu University, Kunshan 215300, China
[c]Department of Internal Medicine of Jiangsu University Hospital Workers, The Affiliated Hospital of Jiangsu University, Zhenjiang 212013, China

†Electronic supplementary information (ESI) available: Supplementary figures (Fig. S1–S5), and a video showing good dispersibility and sprayable behavior of CuO_2 nanodots in water (.mp4). See DOI: 10.1039/d1nr04687j

wounds over the past two decades.[15,16] However, the side effects (such as the increased cancer morbidity) of exogenous growth factors and the high cost of endogenous growth factors limited their widespread application.[17,18] The antibiotics resistance of multidrug-resistant bacteria brought new challenges to infection control in clinics. The protective biofilm (extracellular polymeric substances) generated during bacterial growth prevents antibiotics from entering the wound layer, and ultimately leads to the ineffective antibiotic treatment of diabetic ulcers.[19] Therefore, the development of alternative therapeutic methods that can simultaneously enhance angiogenesis and reduce bacterial infections is highly desirable.

Recently, Lin *et al.* reported the synthesis of CuO_2 nanodots and its application in tumor therapy. According to their report, CuO_2 nanodots were able to decompose into Cu^{2+} and H_2O_2 under weak acidic conditions (pH 5.5), such as in the tumor microenvironment. The hydroxyl radicals ˙OH, an active reactive oxygen species (ROS), would be generated by Fenton-like reaction between Cu^{2+} and H_2O_2, thus achieving an effective anti-tumor activity through ROS.[20] As we all know, both Cu^{2+} and H_2O_2 are acknowledged antimicrobial agents. They have been widely studied and used for the bacterial infection control.[21–25] Compared with antibiotics, Cu^{2+} and H_2O_2 are not hindered by bacterial resistance because it is not easy for the bacteria to produce protective biofilms on their own surfaces.[26,27] In addition, Cu^{2+} was reported to artificially mimic hypoxia in the wound sites, which facilitated the stabi-

lization of hypoxia-inducible factor (HIF-1α) and the expression of downstream-targeted genes, including vascular endothelial growth factor (VEGF), thereby enhancing angiogenesis.[28–30] The Cu^{2+}-incorporated films had been fabricated and employed for wound dressing, displaying improved angiogenesis, antibacterial activity and wound healing.[14] Inspired by these innovative research works, we considered whether CuO_2 nanodots possess the capacities of angiogenesis enhancement and bacteria elimination to accelerate wound healing.

In our concept, CuO_2 nanodots will be decomposed into Cu^{2+} and H_2O_2 under a pathological acidic environment (pH 5.5–5.6) of infected chronic wounds.[31] The released Cu^{2+} and H_2O_2 will effectively inhibit the viability of bacteria, even inhibiting drug-resistant bacteria. Meanwhile, Cu^{2+} will induce enhanced angiogenesis. Benefiting from the dual functions, CuO_2 nanodots will finally realize the therapeutic effect of promoting wound healing in diabetic ulcers (Fig. 1). To validate this concept, herein, CuO_2 nanodots were prepared and their acidic-triggered decomposition into Cu^{2+} and H_2O_2 was confirmed again, according to the pioneer report.[20] The dispersibility of CuO_2 nanodots in water and its sprayable behavior from the spray nozzle were observed. Thereafter, four bacterial strains commonly parasitized in diabetic ulcers were employed, and the *in vitro* antibacterial effect of CuO_2 nanodots was evaluated. Human umbilical vein endothelial cells (HUVECs) were then used for the *in vitro* angiogenesis investi-
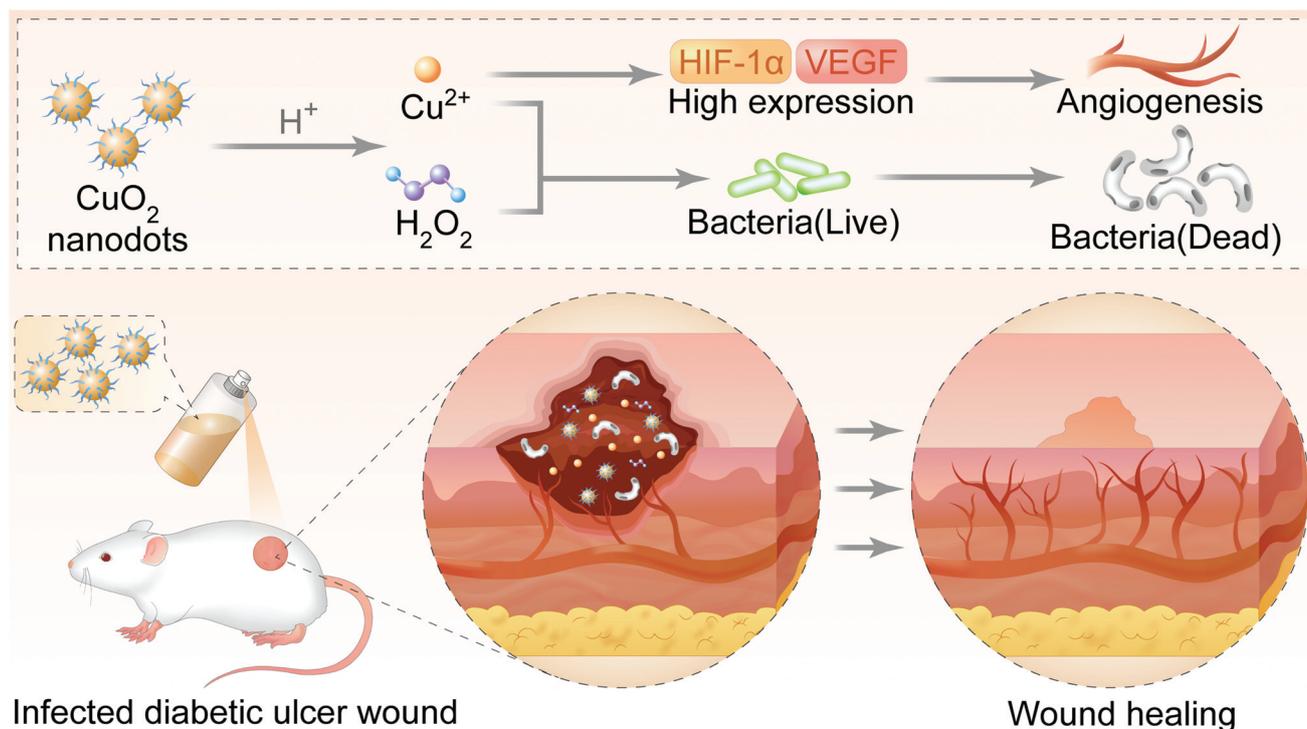

Fig. 1 Schematic illustration of CuO_2 nanodots for accelerating wound healing. After spraying on the diabetic ulcer wound, CuO_2 nanodots can be decomposed into Cu^{2+} and H_2O_2 because of the specific pathological acidic environment (pH 5.5–5.6) in the infected chronic wound. Cu^{2+} and H_2O_2 effectively eliminate bacteria. Cu^{2+} induces the high expression of VEGF and thus promotes angiogenesis. Attributing to the antimicrobial and angiogenesis effects, CuO_2 nanodots accelerate the wound healing in the diabetic ulcer.

gation. The expressions of HIF-1α and VEGF after CuO$_2$ treatment were also quantified. Finally, the methicillin-resistant *Staphylococcus aureus* (MRSA) infected wounds in diabetic mice were created and the wound healing effect was studied. Overall, this paper aims to provide solid evidence for the antimicrobial and angiogenesis abilities of CuO$_2$ nanodots, and try to apply them in the infected wound healing by spray.

Results and discussion

Preparation and characterization of CuO$_2$ nanodots

The CuO$_2$ nanodots were obtained, according to a previous report, by the reaction of CuCl$_2$·2H$_2$O, H$_2$O$_2$ and NaOH in the presence of PVP under stirring for 30 min.[20] As shown in the transmission electron microscopy (TEM) images (Fig. 2B and S1 of ESI, ESI†), there were many ultrasmall black dots, which represented the single CuO$_2$ nanodots. Moreover, these nanodots were clustered and surrounded by irregular nebulosity, probably owing to the PVP coating. In the X-ray photoelectron spectroscopy (XPS) spectra of CuO$_2$ nanodots (Fig. S2A, ESI†), two O 1s peaks at 531.3 and 532.5 eV were assigned to C=O and O–O, respectively, indicating the presence of PVP and peroxo groups. Compared with the spectra of CuO$_2$ synthesized in the absence of PVP (Fig. S2D, ESI†), an obvious N 1s peak was observed in CuO$_2$ nanodots (Fig. S2C, ESI†), further demonstrating the existence of the PVP coating. The hydrodynamic diameter of the CuO$_2$ nanodots was about 7 nm (Fig. 2A). Attributed to the PVP coating and small size, the CuO$_2$ nanodots displayed excellent dispersibility. Even after lyophilization, they could be easily re-dispersed in water and sprayed out from the spray nozzle (Fig. 2C and the video in ESI†). This will be convenient for patients to apply CuO$_2$ nanodots for wound healing. In particular, we noticed that the calcium peroxide (CaO$_2$) nanoparticles were unstable in aqueous solution because of hydrolysis.[32,33] CuO$_2$, as a member of metal peroxides similar to CaO$_2$, seems to be able to hydrolyze in water. Although the hydrolysis might be slight, indicated by the cumulative Cu release in pH 7.4 buffer,[20] CuO$_2$ nanodots should be better preserved in the form of a freeze-dried powder. Subsequently, the excellent redispersibility is crucial for practical application, which allows patients to prepare the spay solution just before use.

In order to confirm the presence of peroxo groups in CuO$_2$ nanodots, the potassium permanganate-based colorimetric method was employed. H$_2$O (control), H$_2$O$_2$, CuO nanoparticles and CuO$_2$ nanodots were mixed with the permanganate (MnO$_4^-$) in acidic solution, respectively. As shown in Fig. 2D, MnO$_4^-$ itself showed a pink color. After mixing with H$_2$O$_2$, the pink color of MnO$_4^-$ faded, owing to the reduction of MnO$_4^-$ to colorless Mn^{2+} by peroxo groups. Similarly, the color of MnO$_4^-$ also faded upon addition of CuO$_2$ nanodots. In contrast, CuO nanoparticles did not cause a color change. Moreover, the spectral absorption curves showed that the absorption peaks of MnO$_4^-$ disappeared after mixing with either H$_2$O$_2$ or CuO$_2$ nanodots. These results demonstrated

the presence of peroxo groups in the CuO$_2$ nanodots. This is consistent with the XPS result. As described above, the O 1s peak at 532.5 eV was assigned to O–O, suggesting the existence of peroxo groups.

Furthermore, we assessed the acid-induced decomposition of CuO$_2$ nanodots into Cu^{2+} and H$_2$O$_2$. As we all know, the Fenton-like reaction between Cu^{2+} and H$_2$O$_2$ will generate a hydroxyl radical (·OH), an active reactive oxygen species (ROS). 3,3′,5,5′-Tetramethylbenzidine (TMB) can be oxidized by ·OH to appear as a blue-green color with maximum absorbance at ~650 nm. As shown in Fig. 2E, neither Cu^{2+} nor H$_2$O$_2$ alone could cause a color change, and result in the detectable absorption peaks of TMB at about 650 nm. By contrast, Cu^{2+} plus H$_2$O$_2$ caused an arresting color change of TMB solution, and produced an absorption peak at 650 nm, thereby confirming the efficient ·OH generation in the presence of Cu^{2+} plus H$_2$O$_2$. Afterwards, CuO$_2$ nanodots were incubated with TMB solutions at pH 7.4 and 5.5, respectively. After incubation for 30 min, the color of the mixture solution displayed an apparent change at pH 5.5, but not at pH 7.4, indicating the ·OH generation under mild acidic (pH 5.5) condition (Fig. 2F). The acidic-induced ·OH generation could be attributed to the decomposition of CuO$_2$ nanodots into Cu^{2+} plus H$_2$O$_2$ under acidic condition and the following Fenton-like reaction between these two decomposition products. Next, we assessed the acid-induced decomposition behavior *via* quantitative measurement of H$_2$O$_2$ generation. As shown in Fig. S3 (ESI†), the cumulative generation of H$_2$O$_2$ at pH 5.5 was always more than the amount at pH 7.4, demonstrating the pH-responsive decomposition of CuO$_2$ nanodots as well. These results demonstrated that CuO$_2$ nanodots were able to release Cu^{2+} and H$_2$O$_2$ at acidic pH, which is exactly beneficial for wound treatment considering the specific pathological acidic environment (pH 5.5–5.6) of the infected chronic wounds.[31]

CuO$_2$ nanodots had been successfully synthesized and carefully characterized by the Chen group. Herein, we examined again the presence of peroxo groups in CuO$_2$ nanodots and their decomposition at acidic pH because both decomposition products (Cu^{2+} and H$_2$O$_2$) were critical to the feasibility of this study. As expected, our results were in good agreement with the characterization by the Chen group, demonstrating again that CuO$_2$ nanodots could release Cu^{2+} and H$_2$O$_2$ at acidic pH. Thereafter, it is reasonable to expect that Cu^{2+} and H$_2$O$_2$ would play the roles for angiogenesis and antibacterial agent, finally promoting the chronic wound healing.

In vitro antibacterial activity

The antibacterial activity of CuO$_2$ nanodots was investigated using four bacterial strain models (*E. coli*, MRSA, *S. aureus* and *P. aeruginosa*), which were the most common bacterial organisms in clinical wound infection. At first, the turbidity and bacterial survival rate were observed by means of the constant broth dilution method. To all of the four bacterial strains, as can be seen in Fig. 3A–D, CuO$_2$ nanodots exhibited dose-dependent antibacterial activity. Along with the increase of the CuO$_2$ concentration, the turbidity of the bacteria medium
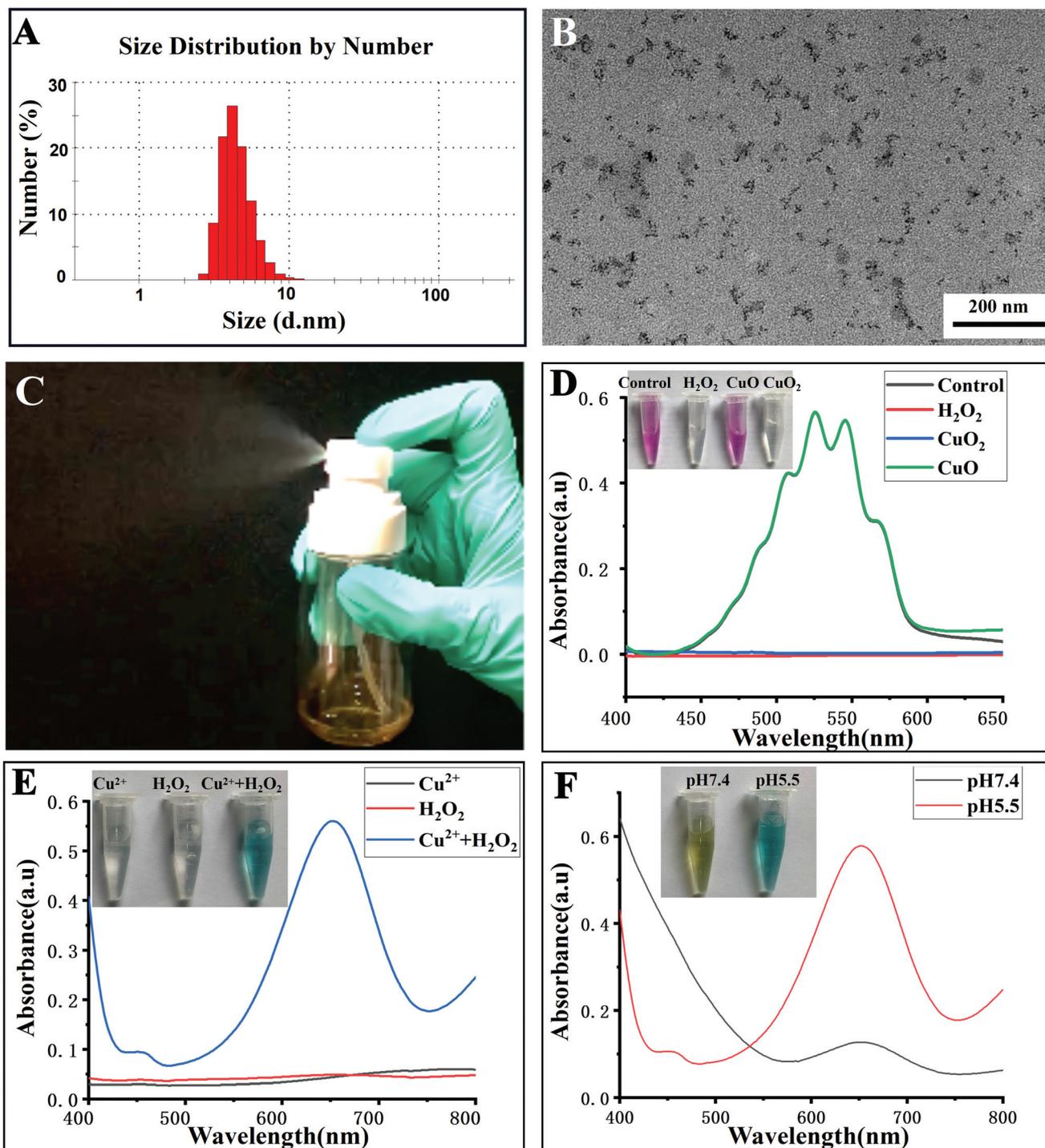
Fig. 2 (A) Hydrodynamic diameter of CuO_2 nanodots measured by dynamic light scattering. (B) TEM images of CuO_2 nanodots. Scale bar = 200 nm. (C) Re-dispersion of CuO_2 nanodots in water after lyophilization and sprayed out from a spray nozzle. (D) Colorimetric analysis demonstrating the presence of peroxo groups in CuO_2 nanodots. (E) Absorption spectrum and photographs (inset) of TMB solution mixing with Cu^{2+}, H_2O_2, or Cu^{2+} plus H_2O_2, respectively. (F) Absorption spectrum and photographs (inset) of the TMB solution mixing with CuO_2 nanodots at different pH values.

decreased gradually, suggesting the enhancement of the bacterial viability inhibition effect.

Subsequently, the colony forming unit plate-counting method was further employed to assess the antibacterial ability. The antibacterial results in all groups (Fig. 4A–D) were in good agreement with the above results obtained by broth dilution method, confirming the dose-dependent antibacterial performance of the CuO_2 nanodots.

Particularly, we noticed that the antibacterial activity against different bacteria was not equivalent. After treatment
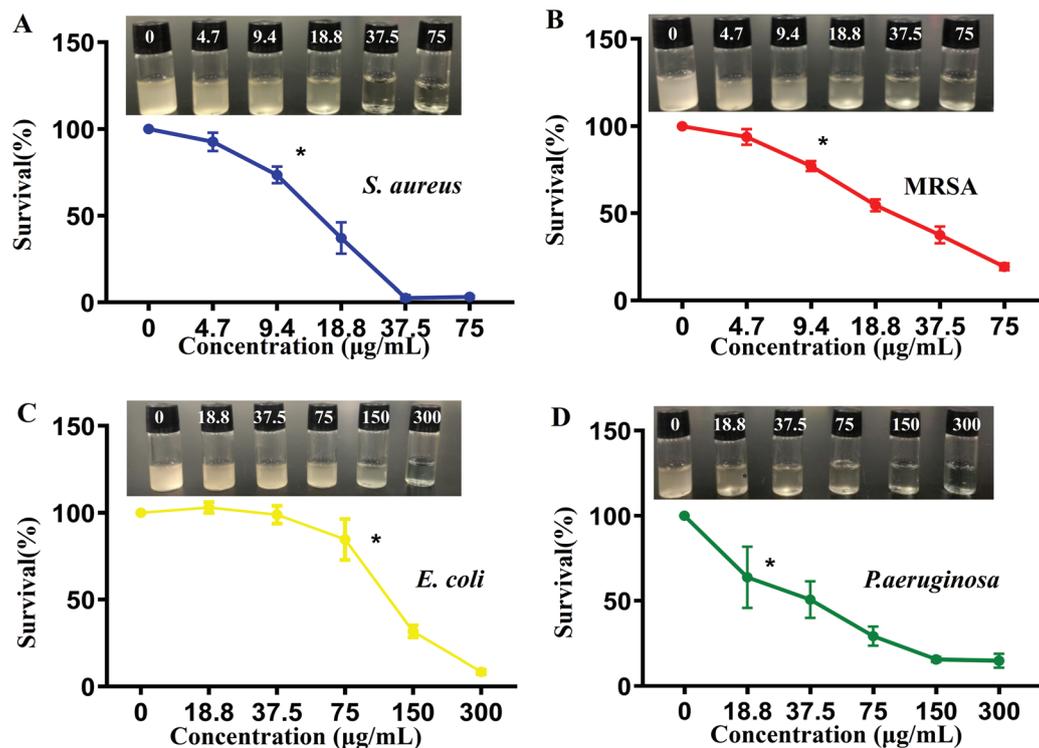
Fig. 3 Antibacterial activity of CuO_2 nanodots at different concentrations *in vitro*. Photographs and survival rates of *S. aureus* (A), MRSA (B), *E. coli* (C) and *P. aeruginosa* (D) after treatment, according to the constant broth dilution method. (*$p < 0.05$).

with CuO_2 nanodots at 37.5 µg mL^{-1}, the survival of *S. aureus* and MRSA declined to 2.6% and 37.5%, respectively, while that of *E. coli* and *P. aeruginosa* remained 95.9% and 50.7% by contrast. It was only when the concentration reached 300 µg mL^{-1} that the survival of *E. coli* and *P. aeruginosa* could decline to 8.7% and 14.8%, respectively. The difference of the antibacterial activity is reasonable because the properties of the four bacterial strains are different. *S. aureus* and MRSA belong to the Gram-positive bacteria, while *E. coli* and *P. aeruginosa* belong to Gram-negative bacteria. According to a previous report, the antibacterial effect of nano-copper particles against Gram-positive bacteria is stronger than Gram-negative bacteria, owing to their differences in the cell wall structure. Copper has high affinity to proteins, while Gram-positive bacteria have more peptidoglycans and proteins on the cell wall, so it is easier to be bound and killed by nano-copper particles.[34]

Generation of reactive oxygen species in bacteria

The reactive oxygen species (ROS) ˙OH will be generated by a Fenton-like reaction between Cu^{2+} and H_2O_2. A previous study had demonstrated that CuO_2 nanodots were able to yield ˙OH in tumor cells because CuO_2 nanodots could be decomposed into Cu^{2+} and H_2O_2 in the acidic endo/lysosomes.[20] Herein, we wish to explore whether the production of ˙OH by CuO_2 nanodots occurs in bacteria as the same. First, the weak acidic microenvironment after bacterial infection was confirmed by the measurement of pH changes in the bacterial suspension.[35]

As shown in Fig. S4 (ESI†), the pH values of culture media with *E. coli*, *S. aureus*, MRSA or *P. aeruginosa* obviously decreased from 7.4 to around 6.5 after 6 h. This result confirmed that the bacteria growth generated an acidic microenvironment, providing the main driving force for the subsequent CuO_2 nanodots decomposition and ROS production. DCFH-DA was employed as the fluorescent ROS indicator, which was nonfluorescent, but could be oxidized by ROS to emit green fluorescence. As can be seen in Fig. 5, barely visible fluorescence was detected in all four bacterial strains without treatment by CuO_2 nanodots. By contrast, all four bacterial strains treated with CuO_2 nanodots present strong fluorescence signal, confirming the production of ROS in bacteria. Considering ROS can damage lipids, proteins and destroy DNA to achieve the bacteria killing,[36–38] we propose the antibacterial effect of CuO_2 nanodots as a result of (a) Cu^{2+} and H_2O_2 themselves from CuO_2 nanodots decomposition, and (b) the ROS generated by the subsequent Fenton-like reaction.

HIF-1α and VEGF expression in HUVECs

In our conception, to achieve the promoted angiogenesis and final wound healing, the Cu^{2+}-induced high expression of HIF-1α and VEGF is crucial to CuO_2 nanodots. Therefore, the HIF-1α and VEGF secretion of HUVECs after incubation with CuO_2 nanodots was investigated using western blot assay. At first, the HUVECs cell viability at different concentrations of CuO_2 nanodots was evaluated to ascertain a suitable concentration range for western blot assay. MTT results (Fig. 6A and
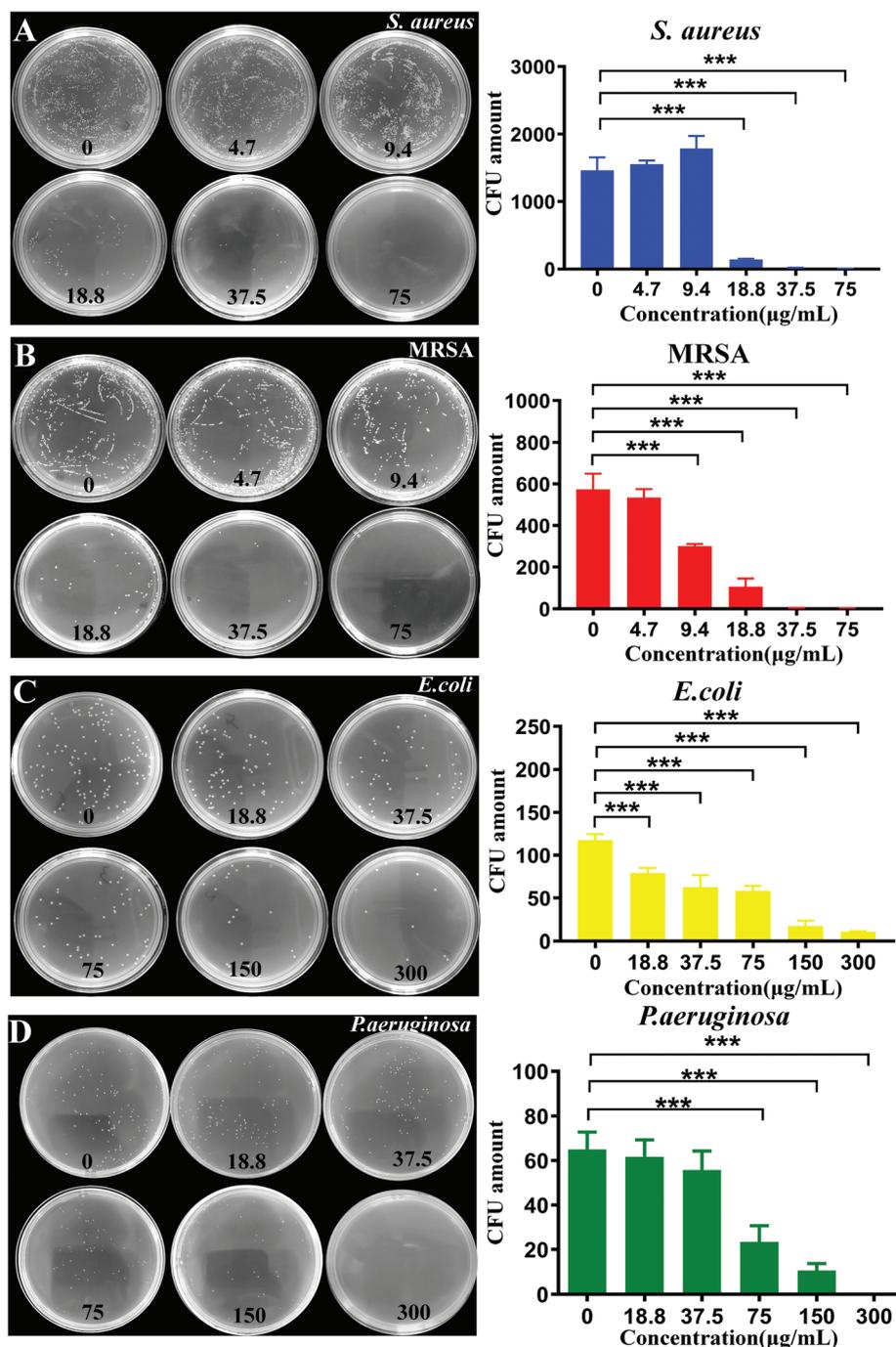
Fig. 4 Antibacterial activity of CuO$_2$ nanodots at different concentrations *in vitro*. Bacterial colonies formed on LB agar plates and the corresponding CFU count of *S. aureus* (A), MRSA (B), *E. coli* (C) and *P. aeruginosa* (D) after treatment, according to the colony forming unit plate-counting method. (*$p < 0.05$, **$p < 0.01$, ***$p < 0.001$).

B) showed that the cell viability was seriously decreased at concentrations of 150 μg mL^{-1} and 300 μg mL^{-1}. When the concentrations were less than 75 μg mL^{-1}, the cell viabilities were all more than 80% at 24 h, and slightly decreased at 48 h. Considering that the bacterial survival rate had been significantly inhibited by the CuO$_2$ nanodots at a concentration of 75 μg mL^{-1} (*$P < 0.05$) in all four bacterial strains (Fig. 3 and

4), we carried out the following studies at the cellular level at concentrations of up to 75 μg mL^{-1}. Fig. 6C displays the protein bands of HIF-1α and VEGF secreted in HUVECs after treatment with CuO$_2$ nanodots at different concentrations. According to statistics, the expressions of both HIF-1α and VEGF were significantly increased at concentrations of 37.5 μg mL^{-1} and 75 μg mL^{-1} (Fig. 6D and E). This must be attributed
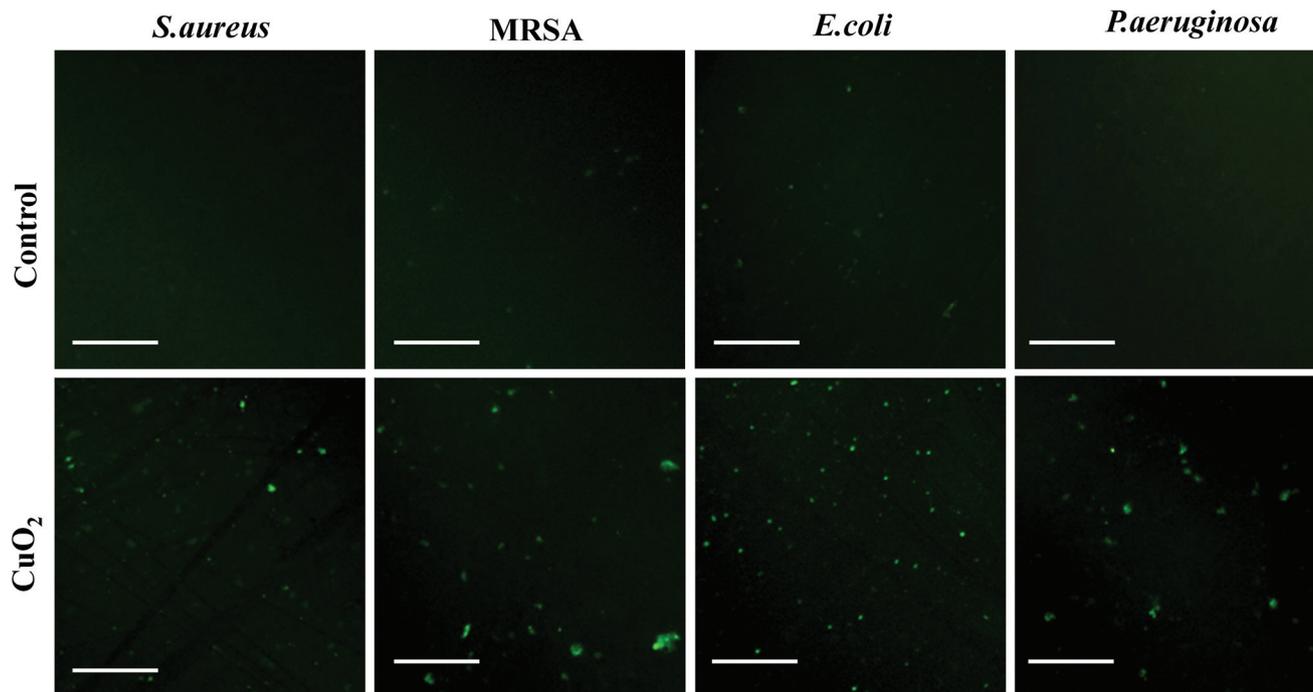
Fig. 5 Fluorescence images of DCFH-DA-stained bacterial strains after treatment without or with CuO_2 nanodots for 3 h. The scale bar represents 100 μm.

to the Cu^{2+} from CuO_2 nanodots because Cu^{2+} had been proven to stabilize HIF-1α and thus inhibit the degradation of HIF-1α, subsequently up-regulating the expression of downstream proteins such as VEGF.[39–41]

Cell migration and tubule formation

As we all known, VEGF is a kind of potent angiogenic cytokine. Since the high expression of VEGF induced by CuO_2 nanodots has been demonstrated as above, the accelerated cell migration was then evaluated by *in vitro* scratch assay and the promoted angiogenesis was investigated by tubule formation assay. In the scratch assay, as shown in Fig. 7A, HUVECs in each group were initially (0 h) slit in the same width. After 48 h of culture, the gaps between scratches were reduced in all research groups, indicating the cells migration. Compared with cells without any treatment, the cells after treatment with CuO_2 nanodots exhibited stronger migration capability, showing an apparently narrower scratches gap. Furthermore, we performed the tubule formation assay on the Matrigel to simulate the angiogenesis of endothelial cells on top of the connective tissue membrane. HUVECs were pretreated with CuO_2 nanodots for 48 h and then inoculated on the Matrigel. After incubation for 3 h, as shown in Fig. 7B, the cells gradually stretched and intersected to form tight junctions, parallel cell lines, branch nodes and mesh circles. All of these are typical indications of the late stage of angiogenesis. By contrast, without pretreatment with CuO_2 nanodots, the cells only formed a few junctions and short lines, suggesting the early stage of angiogenesis. Quantitative analysis of tubule junctions and nodes from different groups were also in agreement with

the microscopic observation, where the groups with CuO_2 nanodots treatment showed an accelerated angiogenesis rate (Fig. 7C and D). This is reasonable because VEGF was highly expressed in HUVECs induced by CuO_2 nanodots at concentrations of 37.5 μg mL^{-1} and 75 μg mL^{-1}, as described in the above western blot assay (Fig. 6D and E).

Accelerated wound healing in diabetic mice

Based on the encouraging antibacterial and angiogenesis results *in vitro*, we investigated the therapeutic effects of CuO_2 nanodots for chronic nonhealing wounds treatment in diabetic mouse models. To evaluate the wound healing efficacy, the wounds with bacterial infection were monitored over time. As shown in Fig. 8A, the wound region in all three groups became smaller with increasing time, and the wounds treated with nanodots healed faster than both control and PVP groups. On day 14, the mice treated with nanodots exhibited the best wound healing, while visible scabs still remained in the other two groups. The wound healing rate curve also indicated that the wound treated with nanodots closed faster than the control and PVP groups (Fig. 8B). After 14 days post-operation, the groups treated with CuO_2 nanodots showed wound healing ratios of 97.5%, significantly higher than that of the control group and PVP group. Notably, considering the existence of PVP in the CuO_2 nanodots, the PVP group was set to explore its influence on the therapeutic effect of CuO_2 nanodots. According to these results, PVP showed negligible effect on wound healing. Thus, the accelerated healing was mainly attributed to the CuO_2 component itself.
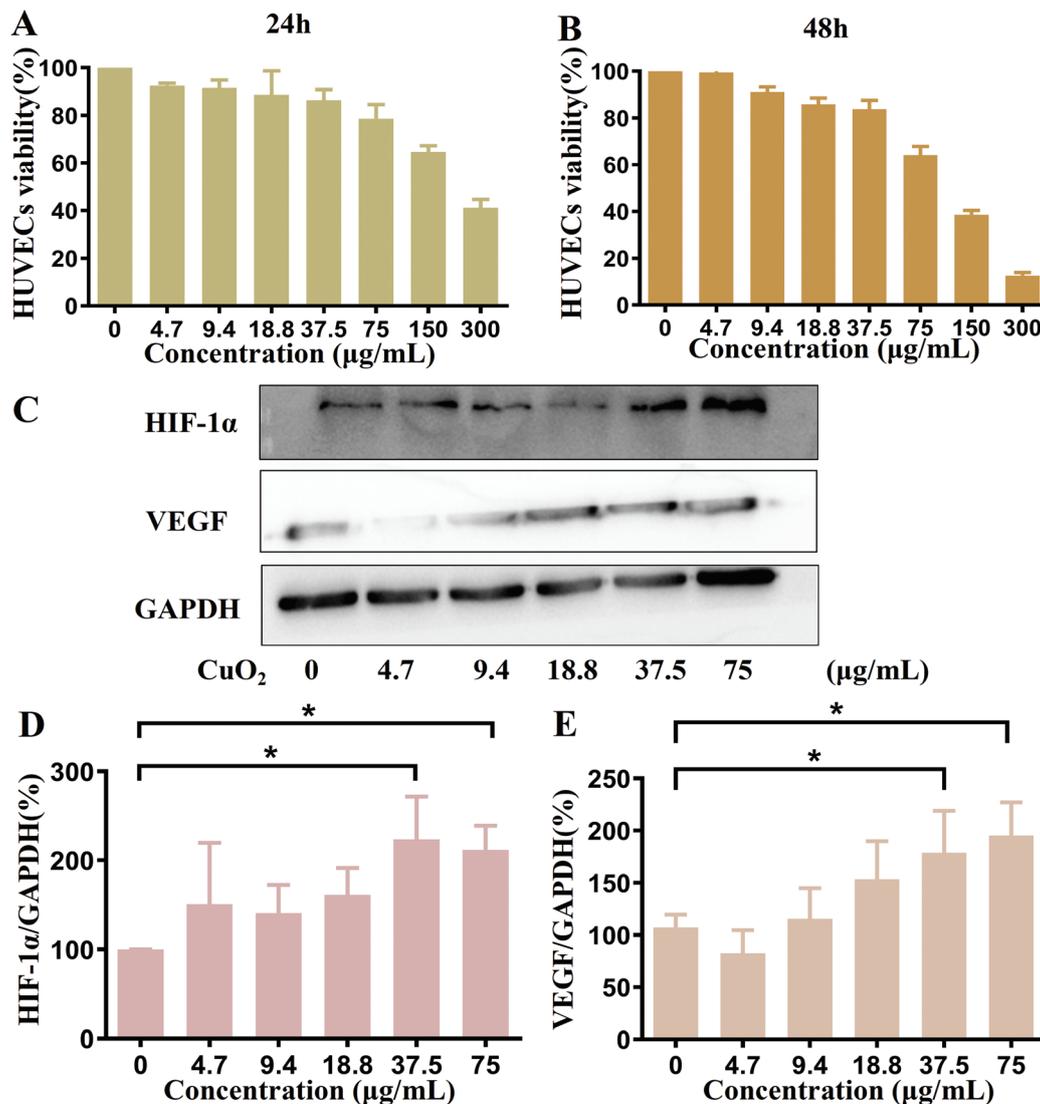
Fig. 6   MTT assay: cell viability of HUVECs treated with CuO_2 nanodots at different concentrations for (A) 24 h and (B) 48 h. Western blot assay: (C) the HIF-1α and VEGF expression of HUVECs after incubation with different concentrations of nanodots; quantification of (D) HIF-1α and (E) VEGF expression by ImageJ.

Wound healing is a complex process. Various biological elements can influence wound healing, such as bacterial infection, inflammation, collagen deposition, angiogenesis and others.[42,43] Hence, Giemsa staining, hematoxylin and eosin (H&E) staining, Masson's trichrome staining and immunohistochemical staining were successively performed to study the potential mechanisms behind the wound healing process generated by CuO_2 nanodots. We described these results as follows:

Bacterial inhibition *in vivo*

In this study, the excisional wounds in diabetic mice were infected by MRSA to establish the bacterial infected wound model. The infected environment is recognized to be able to delay wound healing. Therefore, bacterial infection in different treatment groups was assessed through Giemsa staining. In

both control and PVP groups, large amounts of bacteria were present in the wound bed, while almost no staining bacteria were detected in the CuO_2 nanodots group (Fig. 8C). The bacteria amount in the wound without nanodots treatment was notably higher than that treated with nanodots (Fig. 8D), suggesting the satisfactory antibacterial performance of CuO_2 nanodots *in vivo*.

Reduced inflammation

After MRSA infection, the wound displayed inflammation on day 2. Excessive inflammation is another factor that can delay wound healing. As indicated by H&E staining results (Fig. 9A), the histological slices of the control group and PVP group displayed obvious infiltration of inflammatory cells. In contrast, the infiltration of inflammatory cells was sparsely observed in the wound with CuO_2 nanodots treatment. Quantitative ana-
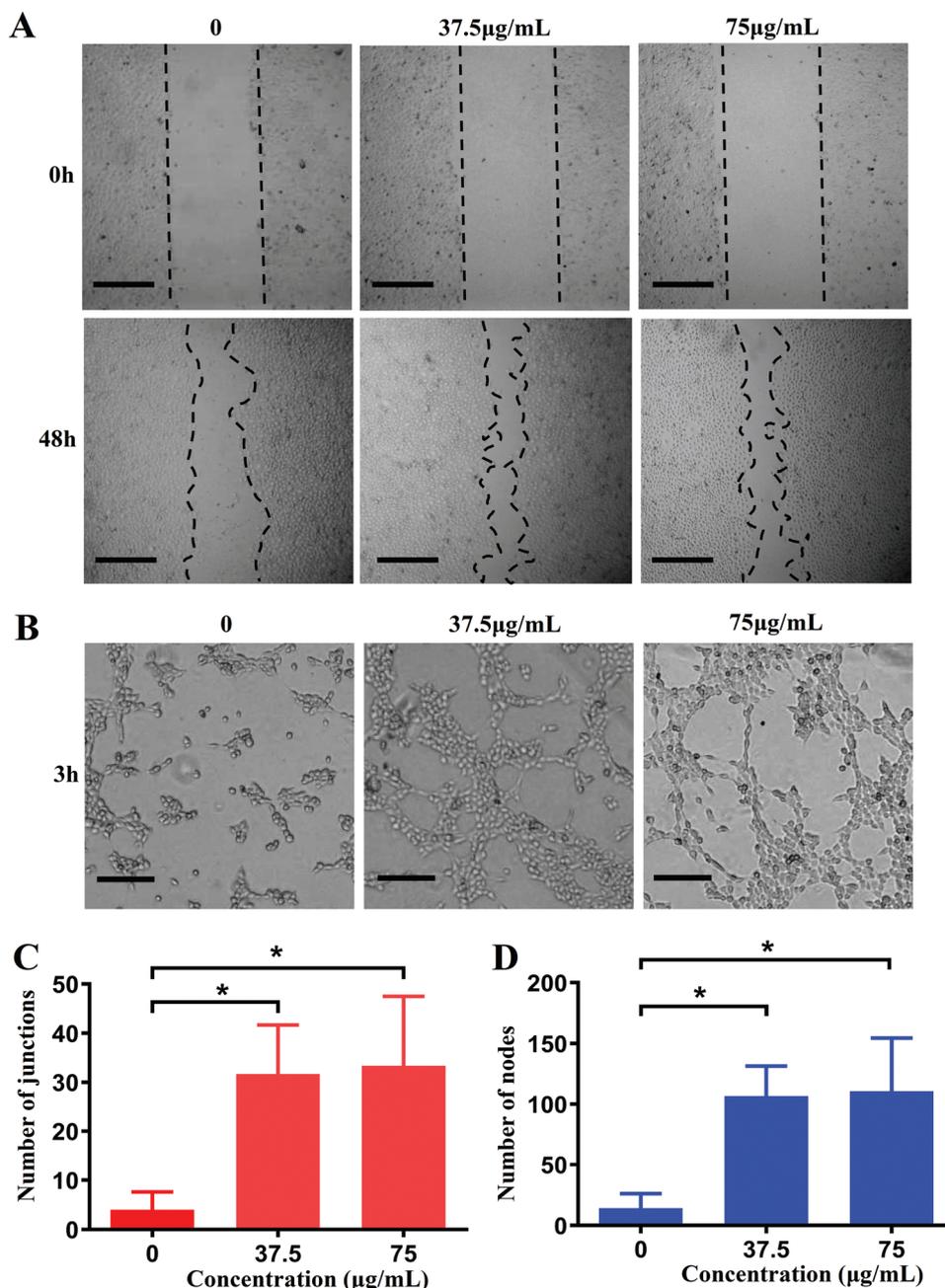
Fig. 7 *In vitro* scratch assay and tubule formation assay. (A) Representative images of scratches healing of HUVECs after treatment with CuO₂ nano-dots for 48 h. Scale bar = 500 μm. (B) *In vitro* tube formation of HUVECs based on the Matrigel. Scale bar = 200 μm. (C) Quantification of tubule junctions by ImageJ. (D) Quantification of tubule nodes by ImageJ.

lysis also suggested that there were significantly fewer inflammatory cells in the CuO₂ nanodots group than the other two groups (Fig. 9B), which may be attributed to the bacterial elimination mediated by CuO₂ nanodots.

Collagen deposition

Collagen fiber is regarded as the extracellular matrix (ECM) remodeling maker. Collagen deposition plays a crucial role in the wound healing process. Herein, Masson's trichrome stain-

ing was performed to analyze the *in vivo* promoting healing effects in terms of the collagen deposition. As the images show in Fig. 9C, compared with the control group and PVP group, more collagen fibers (stained with aquamarine blue) were observed in the CuO₂ nanodots group, and these collagen fibers were interweaved and tended to form network structures. Quantitative analysis of the deposited collagen in the wound region demonstrated that the deposition of collagen in the CuO₂ nanodots group was significantly higher than that in
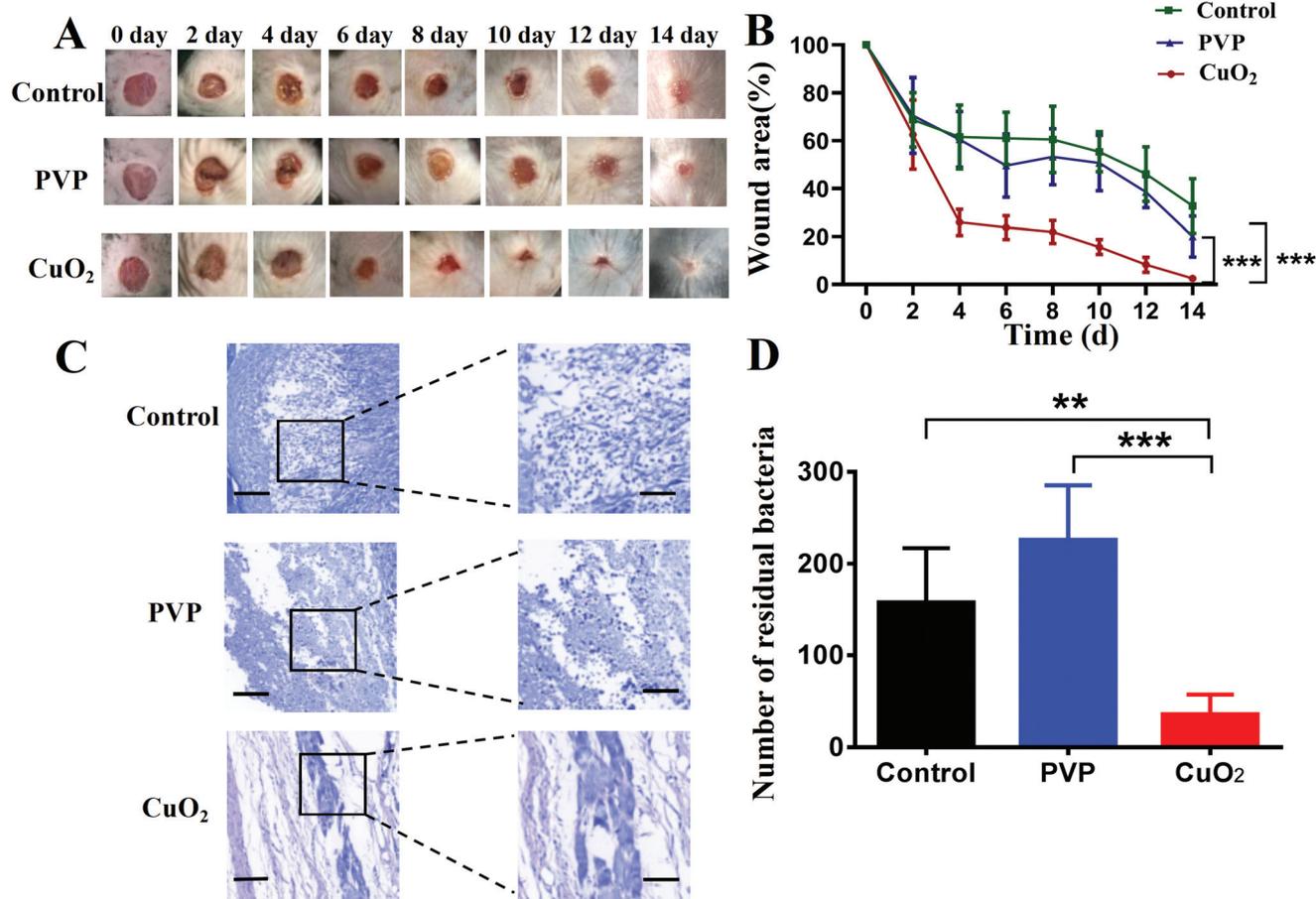
Fig. 8 (A) Overview of the size change of the MRSA infected wounds excised in the dorsal skin at different times after different treatments. (B) Relative wound area curves of mice after different treatments. (C) Giemsa staining of the wound site. Left bar = 100 μm, right bar = 50 μm. (D) Quantitative analysis of the residual bacteria in the wound sites by ImageJ.

the control and PVP groups (Fig. 9D). This might be partially owing to the reduced inflammation mediated by CuO_2 nanodots because the chronic inflammatory stage will generate the overexpression of matrix metalloproteinases, which excessively degrade the ECM component and hinder the collagen deposition.

Promoted angiogenesis

Angiogenesis is essential to wound healing because the healing process needs to transport oxygen and nutrients through the blood into new tissue formation sites. According to our concept, the promoted angiogenesis would be achieved by the high-expression of HIF-1α and VEGF, and indeed we have confirmed their high-expression at the cellular level. Herein, we further evaluated their expression in the wound area *in vivo*. As depicted in Fig. 10A and B, HIF-1α were up-regulated in the wound area after treatment with CuO_2 nanodots, demonstrating higher expression than saline (as control) and PVP treatment. In accordance, its downstream protein VEGF, an important neovascularization factor for wound healing, was also up-regulated in the CuO_2 nanodots group (Fig. 10A and C). This result proved again that the CuO_2 nano-

dots could induce the high expression of HIF-1α and VEGF. Afterwards, to characterize the angiogenesis in wounds, the total number of vessels in a histologic section was investigated by staining with an anti-CD31 antibody. As can be seen in Fig. 10A, there were conspicuous microvessels in the histologic section of the wound treated with CuO_2 nanodots, but sparse blood vessels were found in the control and PVP groups. A significant improvement in the total number of microvessels was counted compared with the other two groups (Fig. 10D), indicating the promoted angiogenesis induced by CuO_2 nanodots.

Taken altogether, these results demonstrate that CuO_2 nanodots effectively achieved eliminated bacteria, reduced inflammation, collagen deposition, promoted angiogenesis, and subsequently accelerated wound healing in diabetic mice.

Pilot toxicity study

Considering that copper is a kind of heavy metal element, which may have potential toxicity to organisms, the toxicity of CuO_2 nanodots to major organs in mice was investigated by H&E staining. The results (Fig. 11) indicated that CuO_2 nanodots, at the therapeutic concentration of 75 μg mL^{-1}, did not show any significant histological changes or toxicity within the
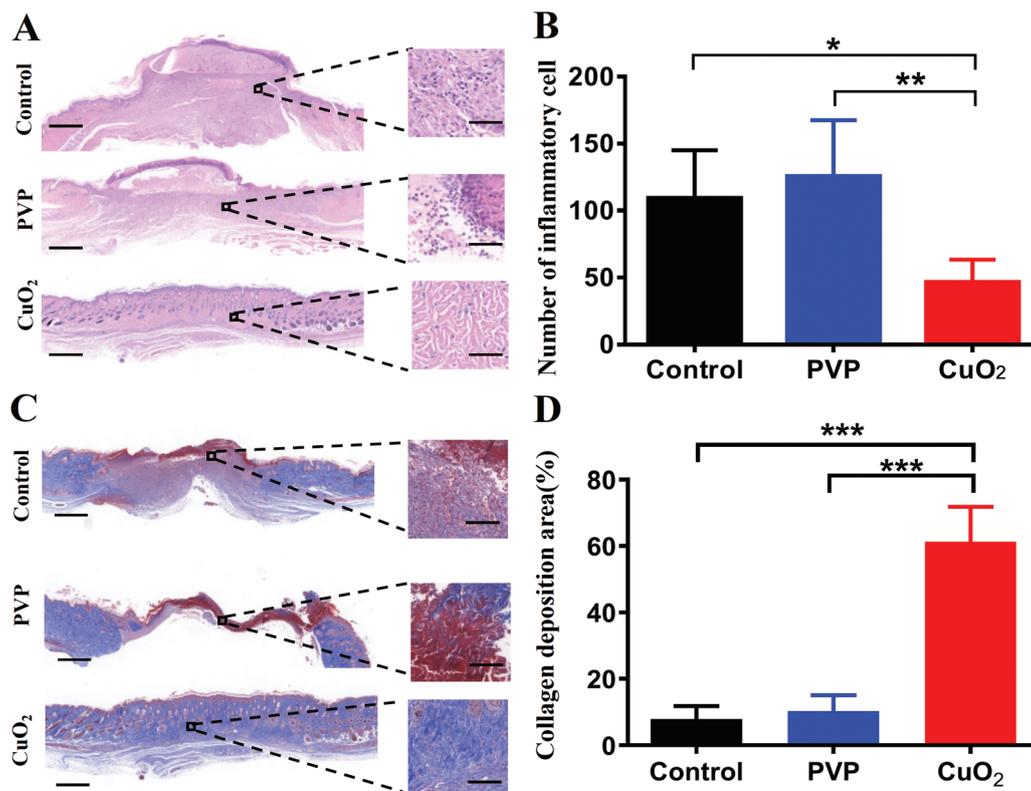
Fig. 9 (A) H&E staining of wound tissue at day 14 after treatment. Left bar = 500 μm, right bar = 50 μm. (B) Quantitative analysis of inflammatory cells in A by ImageJ. (C) Masson staining of the wound tissue. Left bar = 500 μm, right bar = 100 μm. (D) Quantitative analysis of the collagen deposition area in C by ImageJ.

treatment period, suggesting an ideal biocompatibility for the *in vivo* application of antibacterial therapy and wound healing.

Materials and methods

Materials

Escherichia coli (*E. coli*, ATCC 25922), *Staphylococcus aureus* (*S. aureus*, ATCC 25923) and *Pseudomonas aeruginosa* (*P. aeruginosa*, ATCC 9027) were obtained from the Shanghai Bioresource Collection Center (Shanghai, China). Methicillin-resistant *Staphylococcus aureus* (MRSA, ATCC 43300) came from Shanghai Luwei Technology Co., Ltd (Shanghai, China). Human umbilical vein endothelial cells (HUVECs) were supplied by the Cell Bank of the Chinese Academy of Sciences (Shanghai, China).

Copper(II) chloride dehydrate ($CuCl_2 \cdot 2H_2O$), copper oxide (CuO) nanoparticles and 3,3′,5,5′-Tetramethylbenzidine (TMB) were purchased from Aladdin Chemistry Co., Ltd (Shanghai, China). Poly (vinylpyrrolidone) (PVP, M_w 10 000), methyl thiazolyl tetrazolium (MTT), streptozotocin (STZ), antibodies against GAPDH and secondary anti-rabbit IgG were supplied by Sigma-Aldrich Co., Ltd (St Louis, MO, USA). Primary anti-HIF-1α and anti-VEGF antibody were purchased from ImmunoWay Biotechnology (USA). 2′,7′-Dichlorofluorescin diacetate (DCFH-DA) and the bicinchoninic acid assay reagent

(BCA) kit were obtained from Beyotime Biotechnology (Shanghai, China). All other materials in this study, which were of at least reagent grade, were purchased from commercial sources and used as received.

Synthesis and characterization of CuO_2 nanodots

The CuO_2 nanodots were fabricated according to a previous report.[20] Briefly, $CuCl_2 \cdot 2H_2O$ (2.5 mL, 0.02 M) and PVP (2.5 mL, 0.5 g) were mixed under magnetic stirring at room temperature. Thereafter, the above solution was mixed with NaOH (5 mL, 0.02 M) and H_2O_2 (100 μL, 30%), sequentially. After stirring for 30 min, the formed nanodots were collected by ultrafiltration and washed with deionized water at least three times. The obtained CuO_2 nanodots were then lyophilized and stored at 4 °C for further study. The average size of the CuO_2 nanodots was measured with a Zetasizer-ZS90 (Malvern Instruments, Malvern, UK). The morphology of the CuO_2 nanodots was observed using transmission electron microscopy (TEM; Tecnai 12, Philips, the Netherlands).

Colorimetric assay of peroxo groups

$KMnO_4$ (50 μg mL^{-1}) was dissolved in an aqueous H_2SO_4 solution (0.1 M). The acidic $KMnO_4$ solution was then treated with H_2O (as control), H_2O_2, CuO nanoparticles and CuO_2 nano-
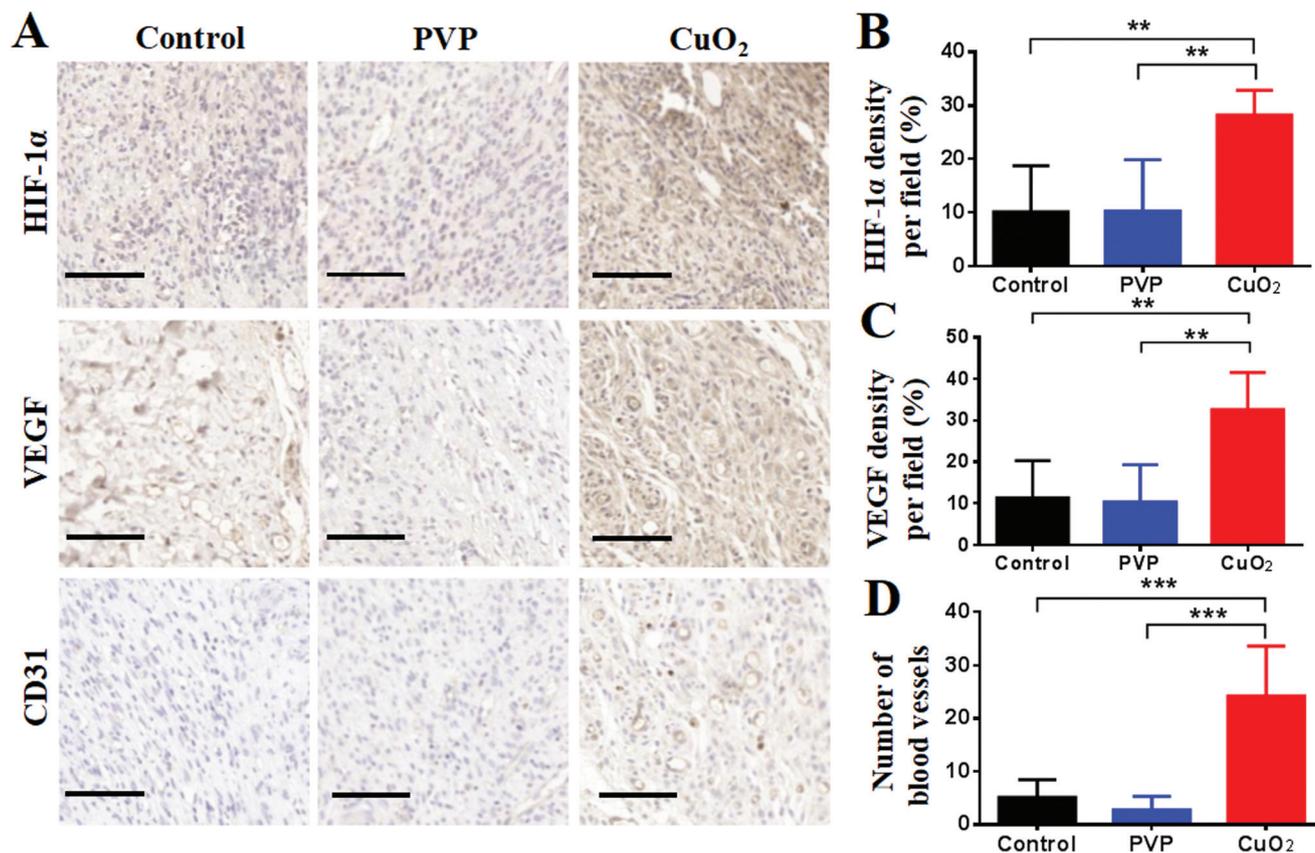
Fig. 10 Immunohistochemical staining (A) and quantitative analysis (B–D) of HIF-1α, VEGF and CD31 in the wound area on day 14 by ImageJ. Scale bar = 100 μm.

dots, respectively. After incubation for 10 min, the UV–Vis spectra were detected from 400 to 650 nm.

Acid-induced decomposition of CuO_2 nanodots into Cu^{2+} and H_2O_2

Taking advantage of the fact that the Fenton-like reaction between Cu^{2+} and H_2O_2 will produce the hydroxyl radical (˙OH), the generation of Cu^{2+} and H_2O_2 after the decomposition of CuO_2 nanodots was examined by detecting the presence of ˙OH. First, the ˙OH generation through the reaction between Cu^{2+} and H_2O_2 was verified by TMB assay. TMB (40 μg mL^{-1}) was dissolved in acetate buffer solution (pH 5.5). Cu^{2+} (1 mM) plus H_2O_2 (1 mM) were mixed with TMB solution. The generation of ˙OH was determined by the obvious absorption peak at 650 nm. TMB solutions mixed with Cu^{2+} and H_2O_2 alone were used as the control groups. Afterwards, CuO_2 nanodots (75 μg mL^{-1}) were mixed with TMB solutions at different pH (5.5 or 7.4). After mixing for 30 min, the photographs of the color changes were taken and the absorption spectra were measured.

In vitro antibacterial effect of CuO_2 nanodots

E. coli, *S. aureus*, MRSA and *P. aeruginosa* were employed to evaluate the antibacterial effects of CuO_2 nanodots *in vitro*. Generally, bacteria in the logarithmic phase were diluted to 10^6

colony-forming units (CFU) per mL, and treated with CuO_2 nanodots at different concentrations (0, 4.7, 9.4, 18.8, 37.5, 75, 150 and 300 μg mL^{-1}). After shaking at 37 °C for 6 h, a 100 μL bacterial suspension from each group was transferred to a sterile 96-well plate. The absorbance was measured at 630 nm using a microplate reader (Bio-Rad, USA). The bacterial survival rates were then further calculated according to the absorbance. Meanwhile, the bacterial suspensions were diluted to 10^3 CFU mL^{-1}, and 50 μL bacterial dilutions were coated on lysogeny broth (LB) agar plates and incubated overnight at 37 °C. The number of bacterial colonies on LB agar plates was counted.

ROS generation in bacteria

Since the hydroxyl radical (˙OH) is an active reactive oxygen species (ROS), we thought that the ROS might be attributed to the antibacterial effect of CuO_2 nanodots. Therefore, we examined the generation of ROS in bacteria after treatment with CuO_2 nanodots. Briefly, CuO_2 nanodots of 75 μg mL^{-1} (in *S. aureus* and MRSA groups) and 300 μg mL^{-1} (in *E. coli* and *P. aeruginosa* groups) were correspondingly mixed with bacterial suspensions, which had been incubated at 37 °C for 3 h. After incubation for another 3 h, bacteria in suspensions were centrifuged and washed twice with PBS to collect bacteria. Afterward, the bacteria were co-cultured with DCFH-DA (10 μM) fluorescent dye at 37 °C for 30 min. After centrifugation and rinse, the bac-
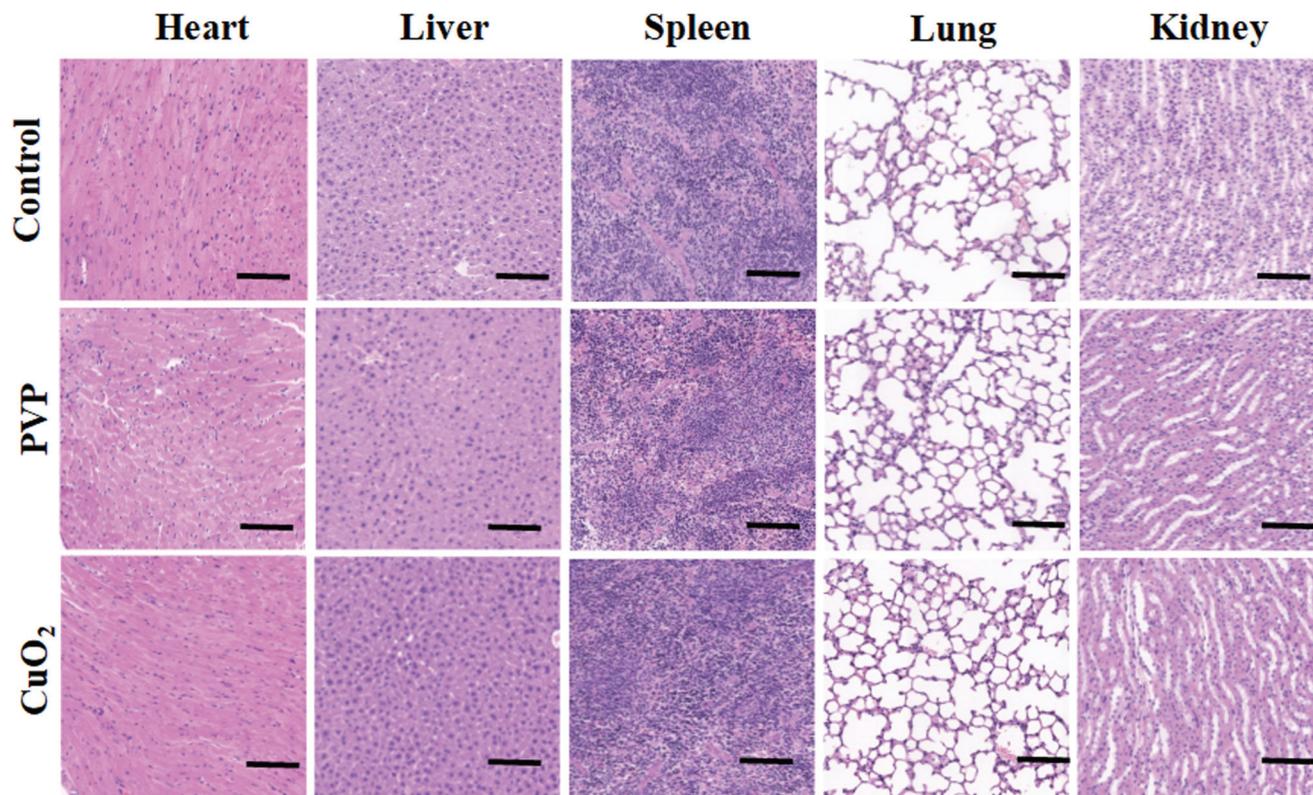
Fig. 11 Histological observation of the H&E staining of major organs in mice after treatment with saline (as control), PVP and CuO₂ nanodots. Scale bar = 100 μm.

teria were harvested and observed by a fluorescence inversion microscope (Olympus Corporation, Japan).

In vitro cytotoxicity

The proliferation of HUVECs after treatment with CuO_2 nanodots was analyzed by MTT test. Briefly, HUVECs were seeded in 96-well plates at 5×10^3 cells per well, and then co-cultured with different concentration series (0, 4.7, 9.4, 18.8, 37.5, 75, 150 and 300 μg mL^{-1}) of CuO_2 nanodots. After 24 h or 48 h incubation, the medium was removed and 10 μL of MTT solution (0.5 mg mL^{-1}) was added in each well. After incubation for 4 h, 150 μL of DMSO was added to each well, and then the absorbance value was measured at 490 nm using a microplate reader (Bio-Rad, USA).

Western blot analysis for HIF-1α and VEGF

HUVECs were treated with different concentrations of CuO_2 nanodots (0, 4.7, 9.4, 18.8, 37.5, 75 μg mL^{-1}) for 48 h, and then lysed in lysis buffer (RIPA lysis buffer containing 1% PMSF) on ice for 15 min. The proteins were collected by centrifugation for 15 min at 4 °C. The protein concentration was decided by BCA kit. Afterwards, equal amounts of heat-denatured proteins were analyzed by 10% SDS-PAGE, then transferred onto PVDF membranes. The membranes were incubated with specific primary antibodies overnight at 4 °C, followed by secondary antibodies. The GAPDH content was used as the loading control. Finally, the signal density of the bands was visualized *via* the MiniChemi Mini Size Chemiluminescent Imaging System (Beijing Sage Creation Science Co., Ltd) and quantified by ImageJ software.

In vitro cell migration

HUVECs were seeded in the 6-well plates (4×10^5 cells per well) overnight to form a confluent monolayer. A straight scratch was then created using a 200 μL tip to mimic an incisional wound. Cells were gently washed with PBS to remove debris. Afterward, the fresh culture medium containing different concentrations of CuO_2 nanodots (0, 37.5 and 75 μg mL^{-1}) were added to each well. After incubation for 48 h, the cells were photographed under a microscope (Olympus Corporation, Japan).

Tubule formation assay

Matrigel was thawed at 4 °C overnight, and then each well of the pre-cooling μ-Slide Angiogenesis (ibidi 81506) was coated with 10 μL matrigel and incubated at 37 °C for 30 min. HUVECs, which had been co-cultured with different concentrations of CuO_2 nanodots (0, 37.5 and 75 μg mL^{-1}) for 48 h, were seeded in each well (10^4 cells) of the pre-processed μ-Slide Angiogenesis. After 3 h of incubation, tubular structures were photographed with a microscope (Olympus Corporation, Japan). The junctions and nodes numbers, which were important parameters for angiogenesis, were quantified using the Angiogenesis Analyzer plugin on ImageJ software.

Diabetic skin wound healing *in vivo*

Six-week-old male C57BL/6J mice were purchased from Nanjing GemPharmatech Co., Ltd. All animal experiments were conducted in accordance with the guidelines specified for laboratory animals by the Ethics Committee of Jiangsu University (Zhenjiang, China). The Animal Care and Use Committee of Jiangsu University approved the use of animals in this study. First, C57BL/6J mice were administered STZ (50 mg kg^{-1}) through intraperitoneal injection for five consecutive days to establish diabetic mellitus-like symptoms.[44,45] The blood glucose levels of the mice were monitored using glucose meters, and the mice with fasted glycemia (8 h fast) < 11.1 mM were excluded (Fig. S5, ESI†). Thereafter, the diabetic mice were anesthetized by 4% chloral hydrate (10 mL kg^{-1}), and a round full-thickness skin wound (diameter: 8 mm) was created on the back of each mouse using biopsy punches. 50 µL of MRSA suspension (10^9 CFU mL^{-1}) was dropped onto the wound immediately to induce diabetic skin infection. These mice were then randomly divided into three groups (*n* = 5), and treated with different therapies: saline (as control), PVP solution (925 µg mL^{-1}) and CuO$_2$ nanodots solution (75 µg mL^{-1}). During the period of treatment, saline, PVP and CuO$_2$ nanodots were sprayed once a day on the wound in corresponding groups. The wound areas were photographed every 2 days and calculated by ImageJ.

Histological analysis

The mice were sacrificed at day 14 post-surgery, and the wounded skins were collected for histological and immunohistochemical staining to evaluate wound healing. Meanwhile, the major organs (heart, liver, spleen, lung, kidney) were excised for hematoxylin and eosin (H&E) staining to study the pilot toxicity of CuO$_2$ nanodots. The tissues (skin specimens and organs from each group) were fixed with 4% paraformaldehyde for 48 h, processed, and embedded in paraffin. The paraffin-embedded tissues were sectioned into 5 µm sections by standard procedures and tiled on the glass slide, followed by deparaffinization and rehydration. Then, H&E staining, Masson's trichrome staining, and Giemsa staining was performed in the skin sections, respectively. The organs sections (including heart, liver, spleen, lung and kidney from each group) were stained by H&E. The pictures were photographed by pathological section scanner (Pannoramic MIDI), and then quantified by ImageJ software.

Immunohistochemical staining was also performed to study angiogenesis in the wound area. In brief, the sections were treated with antigen retrieval using citrate buffer (pH 6.0). The sections blocked with 3% BSA were then incubated with specific primary antibodies against HIF-1α (Servicebio, 1 : 200, GB13031), VEGF (Servicebio, 1 : 500, GB11034) and CD31 (Servicebio, 1 : 1000, GB13428), followed by secondary antibody (Servicebio, 1 : 200 GB23303). For chromogenic staining, 3,3′-Diaminobenzidine (DAB) was used, and then hematoxylin was used as a counterstain. Finally, the images were taken under a pathological section scanner (Pannoramic MIDI) and analyzed by ImageJ software.

Statistical analysis

Origin 8 and GraphPad Prism 9 were applied for all statistical analyses. Statistical analysis was conducted using one-way ANOVA. The results were presented as mean ± SD. Differences between groups were considered statistically significant at *P* < 0.05, and all statistically significant values shown in the figures were indicated as * (*P* < 0.05), ** (*P* < 0.01) or *** (*P* < 0.001).

Conclusions

In summary, we have presented the dispersible and sprayable CuO$_2$ nanodots for the effective treatment of multidrug-resistant bacteria infected diabetic ulcers. After spraying on the infected wound, CuO$_2$ nanodots could be decomposed into Cu^{2+} and H$_2$O$_2$, leading to enhanced antimicrobial and angiogenesis effect. As expected, after treatments with CuO$_2$ nanodots, the viabilities of bacteria (*E. coli*, *S. aureus*, *P. aeruginosa* and MRSA) were significantly inhibited. The cell migration and tube formation were obviously promoted, indicating the activated angiogenesis *in vitro*. Western blot assay showed the high expression of HIF-1α and VEGF in HUVECs, suggesting the potential mechanism of CuO$_2$ nanodots-induced angiogenesis. Consequently, the efficient antibacterial properties and activated angiogenesis ultimately accelerated the wound healing of MRSA-infected diabetic ulcers *in vivo*. Moreover, the cutaneous administration of CuO$_2$ nanodots did not cause systemic toxicity. The results provide sufficient data support for the inherent antibacterial and angiogenesis capacity of CuO$_2$ nanodots, which may greatly expand research areas for CuO$_2$-based materials. Furthermore, the present study offers the applicability of CuO$_2$ nanodots for the treatment of infected wounds by spray for the first time.

Author contributions

Ran Zhang: Data curation, formal analysis, investigation, methodology, validation, writing-original draft; Guhua Jiang: Investigation; Qianqian Gao: Investigation, writing-review & editing; Xiaona Wang: Writing-review & editing; Yilin Wang: Investigation; Xin Xu: Investigation; Wenjing Yan: Investigation; Haijun Shen: Conceptualization, funding acquisition, resources, supervision, writing-review & editing.

Conflicts of interest

The authors declare no conflict of interest.

Acknowledgements

Notes and references

1 N. H. Cho, J. E. Shaw, S. Karuranga, Y. Huang, J. D. da Rocha Fernandes, A. W. Ohlrogge and B. Malanda, *Diabetes Res. Clin. Pract.*, 2018, **138**, 271–281.

2 J. Ouyang, X. Ji, X. Zhang, C. Feng, Z. Tang, N. Kong, A. Xie, J. Wang, X. Sui, L. Deng, Y. Liu, J. S. Kim, Y. Cao and W. Tao, *Proc. Natl. Acad. Sci. U. S. A.*, 2020, **117**, 28667–28677.

3 S. A. Eming, P. Martin and M. Tomic-Canic, *Sci. Transl. Med.*, 2014, **6**, 265sr266.

4 S. Noor, M. Zubair and J. Ahmad, *Diabetes Metab. Syndr.*, 2015, **9**, 192–199.

5 P. C. Leung, *Surgeon*, 2007, **5**, 219–231.

6 P. A. Shiekh, A. Singh and A. Kumar, *Biomaterials*, 2020, **249**, 120020.

7 M. Monteiro-Soares, E. J. Boyko, J. Ribeiro, I. Ribeiro and M. Dinis-Ribeiro, *Diabetes/Metab. Res. Rev.*, 2012, **28**, 574–600.

8 D. F. Bandyk, *Semin. Vasc. Surg.*, 2018, **31**, 43–48.

9 N. Pound, S. Chipchase, K. Treece, F. Game and W. Jeffcoate, *Diabetic Med.*, 2005, **22**, 1306–1309.

10 N. Singh, D. G. Armstrong and B. A. Lipsky, *JAMA*, 2005, **293**, 217–228.

11 R. Nunan, K. G. Harding and P. Martin, *Dis. Models Mech.*, 2014, **7**, 1205–1213.

12 J. M. Smiell, T. J. Wieman, D. L. Steed, B. H. Perry, A. R. Sampson and B. H. Schwab, *Wound Repair Regen.*, 1999, **7**, 335–346.

13 I. B. Wall, C. E. Davies, K. E. Hill, M. J. Wilson, P. Stephens, K. G. Harding and D. W. Thomas, *Wound Repair Regen.*, 2002, **10**, 346–353.

14 J. Li, D. Zhai, F. Lv, Q. Yu, H. Ma, J. Yin, Z. Yi, M. Liu, J. Chang and C. Wu, *Acta Biomater.*, 2016, **36**, 254–266.

15 H. Saad Setta, A. Elshahat, K. Elsherbiny, K. Massoud and I. Safe, *Int. Wound J*, 2011, **8**, 307–312.

16 J. P. Hong, H. D. Jung and Y. W. Kim, *Ann. Plast. Surg.*, 2006, **56**, 394–398; discussion 399–400.

17 U. A. Okonkwo and L. A. DiPietro, *Int. J. Mol. Sci.*, 2017, **18**, 1419.

18 A. P. Veith, K. Henderson, A. Spencer, A. D. Sligar and A. B. Baker, *Adv. Drug Delivery Rev.*, 2019, **146**, 97–125.

19 Y. Qiao, Y. Ping, H. Zhang, B. Zhou, F. Liu, Y. Yu, T. Xie, W. Li, D. Zhong, Y. Zhang, K. Yao, H. A. Santos and M. Zhou, *ACS Appl. Mater. Interfaces*, 2019, **11**, 3809–3822.

20 L. S. Lin, T. Huang, J. Song, X. Y. Ou, Z. Wang, H. Deng, R. Tian, Y. Liu, J. F. Wang, Y. Liu, G. Yu, Z. Zhou, S. Wang, G. Niu, H. H. Yang and X. Chen, *J. Am. Chem. Soc.*, 2019, **141**, 9937–9945.

21 G. Borkow and J. Gabbay, *Curr. Med. Chem.*, 2005, **12**, 2163–2175.

22 A. K. Chatterjee, R. Chakraborty and T. Basu, *Nanotechnology*, 2014, **25**, 135101.

23 S. Jaiswal, P. McHale and B. Duffy, *Colloids Surf., B*, 2012, **94**, 170–176.

24 L. Macomber and J. A. Imlay, *Proc. Natl. Acad. Sci. U. S. A.*, 2009, **106**, 8344–8349.

25 K. Keyer and J. A. Imlay, *Proc. Natl. Acad. Sci. U. S. A.*, 1996, **93**, 13635–13640.

26 S. L. Warnes and C. W. Keevil, *Appl. Environ. Microbiol.*, 2011, **77**, 6049–6059.

27 J. J. Cooney and R. J. Tang, *Methods Enzymol.*, 1999, **310**, 637–644.

28 Z. Zhang, L. Qiu, C. Lin, H. Yang, H. Fu, R. Li and Y. J. Kang, *Metallomics*, 2014, **6**, 1889–1893.

29 T. Himoto, K. Fujita, T. Nomura, J. Tani, H. Miyoshi, A. Morishita, H. Yoneyama, S. Kubota, R. Haba, Y. Suzuki and T. Masaki, *Biol. Trace Elem. Res.*, 2016, **174**, 58–64.

30 A. M. Zimnicka, H. Tang, Q. Guo, F. K. Kuhr, M. J. Oh, J. Wan, J. Chen, K. A. Smith, D. R. Fraidenburg, M. S. Choudhury, I. Levitan, R. F. Machado, J. H. Kaplan and J. X. Yuan, *PLoS One*, 2014, **9**, e90544.

31 J. Wang, X. Y. Chen, Y. Zhao, Y. Yang, W. Wang, C. Wu, B. Yang, Z. Zhang, L. Zhang, Y. Liu, X. Du, W. Li, L. Qiu, P. Jiang, X. Z. Mou and Y. Q. Li, *ACS Nano*, 2019, **13**, 11686–11697.

32 S. Gao, Y. Jin, K. Ge, Z. Li, H. Liu, X. Dai, Y. Zhang, S. Chen, X. Liang and J. Zhang, *Adv. Sci.*, 2019, **6**, 1902137.

33 S. Shen, M. Mamat, S. Zhang, J. Cao, Z. D. Hood, L. Figueroa-Cosme and Y. Xia, *Small*, 2019, **15**, e1902118.

34 M. Tiwari, K. Narayanan, M. B. Thakar, H. V. Jagani and J. Venkata Rao, *IET Nanobiotechnol.*, 2014, **8**, 230–237.

35 B. Tao, Y. Deng, L. Song, W. Ma, Y. Qian, C. Lin, Z. Yuan, L. Lu, M. Chen, X. Yang and K. Cai, *Colloids Surf., B*, 2019, **177**, 242–252.

36 S. Y. Kim, C. Park, H. J. Jang, B. O. Kim, H. W. Bae, I. Y. Chung, E. S. Kim and Y. H. Cho, *J. Microbiol.*, 2019, **57**, 203–212.

37 P. Belenky, J. D. Ye, C. B. Porter, N. R. Cohen, M. A. Lobritz, T. Ferrante, S. Jain, B. J. Korry, E. G. Schwarz, G. C. Walker and J. J. Collins, *Cell Rep.*, 2015, **13**, 968–980.

38 H. Van Acker and T. Coenye, *Trends Microbiol.*, 2017, **25**, 456–466.

39 W. I. Mortada, A. Awadalla, S. Khater, A. Ahmed, E. T. Hamam, M. El-Zayat and A. A. Shokeir, *Environ. Sci. Pollut. Res.*, 2020, **27**, 15835–15841.

40 P. A. Campochiaro, *Prog. Retinal Eye Res.*, 2015, **49**, 67–81.

41 H. Sui, J. Zhao, L. Zhou, H. Wen, W. Deng, C. Li, Q. Ji, X. Liu, Y. Feng, N. Chai, Q. Zhang, J. Cai and Q. Li, *Cancer Lett.*, 2017, **403**, 86–97.

42 E. Vågesjö, E. Öhnstedt, A. Mortier, H. Lofton, F. Huss, P. Proost, S. Roos and M. Phillipson, *Proc. Natl. Acad. Sci. U. S. A.*, 2018, **115**, 1895–1900.

43 Y. Zhu, Z. Cankova, M. Iwanaszko, S. Lichtor, M. Mrksich and G. A. Ameer, *Proc. Natl. Acad. Sci. U. S. A.*, 2018, **115**, 6816–6821.

44 J. Gan, C. Liu, H. Li, S. Wang, Z. Wang, Z. Kang, Z. Huang, J. Zhang, C. Wang, D. Lv and L. Dong, *Biomaterials*, 2019, **219**, 119340.

45 X. Ren, Y. Han, J. Wang, Y. Jiang, Z. Yi, H. Xu and Q. Ke, *Acta Biomater.*, 2018, **70**, 140–153.